2023 IEEE International Conference on Robotics and Automation (ICRA 2023)
May 29 - June 2, 2023. London, UK

External Force Estimation of Legged Robots via a Factor Graph Framework with a Disturbance Observer

Jeonguk Kang[1] Hyun-Bin Kim[1] Keun Ha Choi[2] and Kyung-Soo Kim[1]

Abstract— **Recently, legged robots have been used for various purposes, such as exploring unknown terrain or interacting with the world. For control and planning legged systems during interactive operations, it is essential to estimate and respond to external forces. However, in legged system, it becomes difficult to estimate forces due to highly dynamic situations. There are several studies that use a force sensor on the foot and end effector, but these approaches have disadvantages in terms of cost and sustainability. Therefore, in this paper, we propose an improved method for estimating external forces without a force sensor. First, each leg force was obtained using the system dynamics of the robot with a disturbance observer. Then, by preintegration, it was tightly coupled with other sensors to estimate the pose and external force simultaneously. Despite the impact and slip, we estimate external forces accurately in standing and walking motions. Moreover, we compared pose estimation performance with VINS-Mono [1], and there is no significant accuracy degradation in spite of highly dynamic force residual.**

I. INTRODUCTION

Currently, many mobile platforms are being used for exploration, delivery, and interaction. To perform these tasks, the estimation of external forces is a very important issue, especially in legged robots. The robot should be able to maintain balance and operate in response to disturbances. These forces can be easily obtained using a force sensor, but most of them are expensive and heavy. Moreover, it can only be measured by attaching them to the exact location in which the force is applied. In particular, to obtain the ground reaction force, which is one of the external forces applied to the robot, a force sensor is usually attached to the tip of the foot. However, when an impact occurs during contact change, the sensor will be accompanied by a large amount of noise and may damage the sensor. Therefore, if it is possible to estimate the external force without a force sensor in a legged robot, it will have a great advantage in terms of maintenance and cost.

Studies estimating the pose or external force of a legged robot have been conducted using several filtering-based methods. The extended Kalman filter was used on a legged robot for pose estimation [1]–[3]. In addition, forces in legged robots or manipulators have also been estimated using filtering-based methods [4]–[6]. These methods are relatively inaccurate compared to the optimization method due to the inherent linearization error. Also, if the number of observation variables increases, estimation performance could become unstable.

On the other hand, factor graph optimization has been used in recent years due to improvements in computing performances. This optimization based method is generally more accurate than the filtering based method and can consider the noise characteristics of all sensors at the same time. For pose estimation, a state-of-the-art visual inertial odometry (VIO), VINS-Mono [7] and ORB-SLAM3 [8], were developed and showed high performance. These can tightly fuse the IMU, which is a high-frequency sensor, due to the IMU preintegration theory [9]. After this theory was presented, it was used variously in legged robots. There are studies that consider preintegrated contact factors and forward kinematics [10], and [11] describes a velocity bias estimation with preintegration.

However, most of the studies on VIO and the aforementioned studies do not use system dynamics. In fact, since dynamics are dependent on the state of the robot, they can be integrated if additional residuals are properly configured. That is, by using the relationship between the force (generated by the actuator) and the state, the applied external force can be estimated. Related studies are VIMO [12] and VID-Fusion [13]. These studies measure the actuator force of micro aerial vehicles (MAVs), obtain a dynamic model, and finally estimate disturbances with robot states based on factor graph approaches.

In this paper, we propose a method of external force estimation using a factor graph in a legged system, specifically a quadruped system. Unlike in the VIMO [12] and VID-Fusion [13] studies, in a legged system, the ground reaction force generated by the actuator is not continuous and is affected by the contact condition while walking. Therefore, it is necessary to more accurately calculate the ground reaction force generated by the robot. Thus, we construct system dynamics and a disturbance observer to obtain the leg forces. Afterward, we tightly couple the results with the other sensors: an IMU and a stereo camera. Finally, pose and external forces can be estimated simultaneously.

This paper is organized as follows. In Section 2, we introduce how to estimate the ground reaction force. In Section 3, we describe the estimation of external forces with a factor graph framework. In Section 4, simulations are conducted to verify the proposed method, and the results

*This research was supported by a grant from Technology Program funded by KHNP(Korea Hydro & Nuclear Power), and the Institute of Civil Military Technology Cooperation funded by the Defense Acquisition Program Administration and Ministry of Trade, Industry and Energy of the Korean government under grant No. 19-CM-GU-01.

[1]J. Kang, H.-B. Kim and K.-S. Kim are with the Department of Mechanical Engineering, Korea Advanced Institute of Science and Technology (KAIST), Deajeon, South Korea. kju2556@kaist.ac.kr

[2] K. Choi is with the Daedong-KAIST Research Center for Mobility, Daejeon, South Korea. choiha99@kaist.ac.kr

are analyzed. Finally, in Section 5, we provide a conclusion and future works.

II. GROUND REACTION FORCE ESTIMATION

In this section, we obtained the ground reaction force of each foot more accurately based on the robot dynamics and disturbance observer. First, the system dynamics configuration will be introduced, and then the disturbance observer (DOB) configuration will be explained.

A. Quadruped dynamic model

Legged robots are usually described with floating base dynamics. In particular, the quadruped robot has a total of 18 DOFs by combining 6 DOFs (x, y, z, roll, pitch, yaw of the base) and 12 actuated joints. Therefore, to represent the quadruped system used in this study, the overall dynamics were obtained as shown in Equation (1). $M(q)$ is the 18×18 inertia matrix, $h(q,\dot{q})$ is the 18×1 coriolis and gravitational term, J_{ci} is the 3×18 contact jacobian of the i^{th} leg, S is the 12×18 selection matrix, τ denotes 12×1 each joint torque, and finally, J_{ext} and F_{ext} denote the 3×18 external force contact jacobian and 3×1 force applied to the base. Additionally, the $q_i, \dot{q}_i$ used to calculate each matrix is the 18×1 generalized position and velocity of the system.

$$M(q)\ddot{q}+h(q,\dot{q})=S^T\tau+\sum_{i=1}^{4}(J_{ci}^T F_{leg,i})+J_{ext}^T F_{ext} \quad (1)$$

Meanwhile, in this study, we focused on the case where an external force was applied to the robot base. Thus, we only need to analyze the 7^{th} to 18^{th} columns of (1).

$$M_i(q_i)\ddot{q}_i+h_i(q_i,\dot{q}_i)=\tau_i+(J_{ci}^T F_{leg,i}) \quad (2)$$

The dynamic equation of the i^{th} leg is described as (2). This expression was constructed by extracting only the rows related to the i^{th} leg in (1). For convenience, $J_{ci}^T F_{leg,i}$, the last term in (2), is defined as τ_{ext}. When this value is obtained, the ground reaction force can also be calculated through the inverse matrix of J_{ci}^T. Solving (2) for τ_{ext} implies $\tau_{ext} = M_i(q_i)\ddot{q}_i + h_i(q_i,\dot{q}_i) - \tau_i$. Here, the value $\ddot{q}$ is the second derivative of the encoder measurement, which can result in a very noisy signal. To solve this issue, $\ddot{q}_i$ was calculated through centered window differentiation in [14], and in other studies, the modeling was simplified, and related terms were neglected. However, when highly dynamic motion occurs, we may need to use an excessive filter, which can lead to poor results. Therefore, we adopt the DOB-based approach [15], which is a method that does not use $\ddot{q}_i$ directly.

B. Nonlinear disturbance observer

Here, we will briefly explain the DOB presented in [15]. The DOB equation for estimating τ_{ext} is shown as (3). G_i is the gain of the DOB, and the $\hat{()}$ operator indicates the estimated value.

$$\dot{\hat{\tau}}_{ext,i}=-G_i\hat{\tau}_{ext,i}+G_i(M_i(q_i)\ddot{q}_i+h(q_i,\dot{q}_i)\dot{q}_i-\tau_i) \quad (3)$$

$$\begin{aligned}\dot{\tilde{\tau}}_{ext,i}&=\dot{\tau}_{ext,i}-G_i\tilde{\tau}_{ext,i}\\ where\ \tilde{\tau}_{ext,i}&=\tau_{ext,i}-\hat{\tau}_{ext,i}\end{aligned} \quad (4)$$

We defined the observer error as $\tilde{\tau}_{ext,i}=\tau_{ext,i}-\hat{\tau}_{ext,i}$, and this error dynamics is shown in (3). Through this equation, we can confirm that the value of τ_{ext} can be estimated to be exponentially stable. However, (3) is dependent on the value of $\ddot{q}_i$, which leads to very noisy and inaccurate results. In [15], the problem was solved using an auxiliary variable.

$$\begin{aligned}z_i&=\hat{\tau}_{ext,i}-H(q_i,\dot{q}_i)\\ where\ \tfrac{d}{dt}H(q_i,\dot{q}_i)&=G_iM_i(q_i)\ddot{q}_i\end{aligned} \quad (5)$$

The nonlinear DOB equation was modified by defining the auxiliary vector $H(q,\dot{q})$. The new expression is expressed as (6) without the $\ddot{q}_i$ term.

$$\dot{z}_i=-G_iz+G_i(h_i(q_i,\dot{q}_i)\dot{q}_i-\tau_i-H(q_i,\dot{q}_i)) \quad (6)$$

After obtaining the z_i value through the above equation, the estimated value of τ_{ext} can be calculated through the definition (5). Meanwhile, to construct the DOB equation, the gain value G_i and the auxiliary matrix $H(q,\dot{q})$ value should be appropriately obtained as (7). A more detailed explanation is given in [15], so we did not provide additional explanations in this section.

$$G_i=X_i^{-1}M_i^{-1}(q_i),\ H(q_i,\dot{q}_i)=X_i^{-1}\dot{q}_i \quad (7)$$

III. FACTOR GRAPH FOR EXTERNAL FORCE ESTIMATION

In this section, we describe the factor graph formulations based on VINS-Mono [7], VIMO [12], and VID-Fusion [13]. External force residuals and leg odometry residuals were added to the existing visual-inertial odometry (VIO), and the overall diagram is illustrated in Fig. 1.

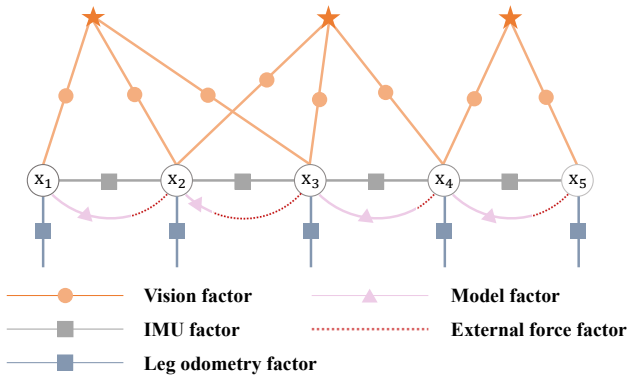

Fig. 1: Factor graph structure with various factors. It consists of the vision factor, model factor, IMU factor, external force factor and leg odometry factor.

A. Formulation

The state vector used in this study is shown in (8), and the sliding window consists of n robot states and m inverse depths of features. x_k is composed of $p^w_{b_k}, v^w_{b_k}, q^w_{b_k}, b_a, b_w, f^{b_k}_{ext}$ as in the second line, where each term is defined as the relative position in b_k frame to world coordinate. Each represents velocity, orientation, acceleration bias, gyroscope bias, and external force.

$$\begin{aligned} \chi &= [x_0, x_1, \dots x_{n-1}, \lambda_0, \lambda_1, \dots \lambda_m] \\ x_k &= [p^w_{b_k}, v^w_{b_k}, q^w_{b_k}, b_a, b_w, f^{b_k}_{ext}], \quad k \in [0, n] \end{aligned} \tag{8}$$

The whole objective function constructed to obtain the maximum posterior estimate for χ is:

$$\begin{aligned} \min_{\chi} \Bigg\{ &||r_p||^2 + \sum_{k\in B} ||r^k_B||^2_{W^k_B} + \sum_{(i,j)\in B} \rho(||r^{l,j}_C||^2_{W^{l,j}_C}) \\ &+ \textstyle\sum_{k\in B} ||r_{LO}||^2_{W^k_{LO}} + \sum_{k\in F} ||r^k_F||^2_{W^k_F} \Bigg\} \end{aligned} \tag{9}$$

where r_p, r_b, r_c are the prior/inertial/visual residuals, and r_{LO}, r_F are the leg odometry and external force residuals. B, C, and F indicate robot state/feature/external force measurements in the sliding window. Additionally, $W^k_B, W^{i,j}_C, W^k_{LO}, W^k_F$ is the corresponding information matrix of each residual.

B. Residual of leg odometry

Because a legged robot can utilize kinematic information, a leg odometry residual is also added, as shown in r_{LO} of (9). If the contact of each leg is maintained between Frame i and Frame j, we can assume that the end effector does not move, and we can construct a residual through the relationship (10).

$$\begin{aligned} r_{LO} &= LO_j - \hat{p}^b_{e,j} \\ &= LO_j - (\hat{R}^w_{b,j})^T(\hat{p}^w_{e,j} - \hat{p}^w_{b,j}) \\ &= LO_j - (\hat{R}^w_{b,j})^T(\hat{p}^w_{e,j} - \hat{p}^w_{b,i}) \\ &= LO_j - (\hat{R}^w_{b,j})^T(\hat{R}^w_{b,i} LO_i + \hat{p}^w_{b,i} - \hat{p}^w_{b,j}) \end{aligned} \tag{10}$$

LO_k is the position from the body to the foot, which is obtained through forward kinematics. R^w_b, p^w_b represents the orientation and pose estimation values of the robot state in the world coordinate. p^b_e, p^w_e is the end effector position of the robot from the body and world frame, respectively. If the contact between the i^{th} frame and the j^{th} frame is maintained, the second line can be converted tothe third line in the equation.

C. Preintegration of external force

1) External force with model dynamics: Before constructing the external force residual, we try to obtain a relational expression through the robot dynamics. For convenience, we assumed that the center of gravity of the entire system is the center of the base. This can be approximated because the mass of the robot leg is relatively smaller than the base. The force applied to the robot includes the gravity, external force and leg forces generated by each foot. $\hat{a}^b$ and b_a are the measurement of acceleration and bias, n_a and n_{leg} represent the noise of the IMU and estimated leg force, respectively. The whole equation is expressed as follows:

$$\begin{aligned} Ma^b &= R^b_w \sum_{i=1}^{4} F_{leg,i} + F^b_{ext} - R^b_w g^w - M n_{leg} \\ &= M(\hat{a}^b - b_a - R^b_w g - n_a) \end{aligned} \tag{11}$$

Finally, the above formula is rearranged for F^b_{ext} as follows:

$$F^b_{ext} = (M(\hat{a}^b - b_a) - R^b_w \sum_{i=1}^{4} F_{leg,i}) - M(n_a - n_{leg}) \tag{12}$$

2) Preintegration with external force: Since the external force obtained above is a high-frequency sensor input similar to the IMU, it can be tightly coupled through the preintegration method. That is, as in the case of the IMU, sensor measurements are expressed as one factor by integrating the ground reaction forces between frames. If integration is performed for the local frame b_k between b_k and b_{k+1}, the following expression can be obtained:

$$\begin{aligned} \hat{\alpha}^{b_k}_{b_{k+1}} &= \iint_{t\in[t_k,t_{k+1}]} R^{b_k}_t (\frac{1}{M} \sum_{i=1}^{4} F^{b_t}_{leg,i} - n_{leg}) \delta t^2 \\ \hat{\beta}^{b_k}_{b_{k+1}} &= \int_{t\in[t_k,t_{k+1}]} R^{b_k}_t (\frac{1}{M} \sum_{i=1}^{4} F^{b_t}_{leg,i} - n_{leg}) \delta t \\ \hat{\psi}^{b_k}_{b_{k+1}} &= \frac{1}{t_{k+1} - t_k} \int_{t\in[t_k,t_{k+1}]} R^{b_k}_t (\frac{1}{M} F^{b_t}_{ext}) \delta t \\ \hat{\gamma}^{b_k}_{b_{k+1}} &= \int_{t\in[t_k,t_{k+1}]} \frac{1}{2} \Omega(\hat{\omega}^b_t - b_{w_t} - n_w) \hat{\gamma}^{b_k}_t \delta t \end{aligned} \tag{13}$$

As shown in (13), α and β have the same form as in the IMU preintegration, and they are configured by replacing the acceleration value with the leg force input. In addition, the newly added ψ indicates the average external force value between b_k and b_{k+1}.

Next is the propagation of the external force. Similar to the IMU, the propagation of α, β, and γ proceeds, and the newly added term ψ is described as in the third row according to (14). During propagation, the bias values b_a and b_w are assumed to be constant. $F^{b_i}_{leg,j}$ is obtained according to the rate of the measurement in the motor, and $\hat{a}^{b_i}$ is updated with the IMU rate. Finally, propagation is performed according to the faster rate sensor.

$$\begin{aligned} \hat{\alpha}^{b_k}_{i+1} &= \hat{\alpha}^{b_k}_i + \hat{\beta}^{b_k}_i \delta t + \frac{1}{2} R^{b_k}_i (\sum_{j=1}^{4} F^{b_i}_{leg,j}) \delta t^2 \\ \hat{\beta}^{b_k}_{i+1} &= \hat{\beta}^{b_k}_i + R^{b_k}_i (\sum_{j=1}^{4} F^{b_i}_{leg,j}) \delta t \\ \hat{\psi}^{b_k}_{i+1} &= \hat{\psi}^{b_k}_i + R^{b_k}_i (\hat{a}^{b_i} - b_{a_k} - \sum_{j=1}^{4} F^{b_i}_{leg,j}) \delta t \\ \hat{\gamma}^{b_k}_{i+1} &= \hat{\gamma}^{b_k}_i \otimes \begin{bmatrix} 1 \\ \frac{1}{2}(\omega^{b_i} - b_{w_k}) \delta_t \end{bmatrix} \end{aligned} \tag{14}$$

Meanwhile, the error state for discrete time propagation is defined as in (15). Then, in (16), the covariance $P_i^{b_k}$ is obtained by linearizing the error state, where n is a noise vector with $n = [n_{leg}, n_w, n_{b_w}, n_a, n_{b_a}]^T$. F_i and G_i are the state transition matrix of the error state and noise-related matrix, respectively. A detailed explanation of the derivation process can be found in [16]. The propagation formula is constructed as follows:

$$\delta z = [\delta\alpha, \delta\beta, \delta\psi, \delta b_a, \delta b_w] \tag{15}$$

$$\begin{aligned} \delta z_{i+1}^{b_k} &= F_i \delta z_i^{b_k} + G_i n \\ P_{i+1}^{b_k} &= F_i P_i^{b_k} F_i^T + G_i Q G_i^T \\ with \quad F_i &= \frac{\partial z_{i+1}^{b_k}}{\partial z_i^{b_k}} \; and \; G_i = \frac{\partial z_{i+1}^{b_k}}{\partial n} \end{aligned} \tag{16}$$

Each bias is assumed to be constant during propagation. If the bias changes slightly, it can be approximated through the first-order Jacobian approximation. The bias approximation is represented by:

$$\begin{aligned} \hat{\alpha}_{b_{k+1}}^{b_k} &= \hat{\alpha}_{b_{k+1}}^{b_k} + J_{b_w}^{\alpha} \delta_{b_{w_k}} \\ \hat{\beta}_{b_{k+1}}^{b_k} &= \hat{\beta}_{b_{k+1}}^{b_k} + J_{b_w}^{\beta} \delta_{b_{w_k}} \\ \hat{\psi}_{b_{k+1}}^{b_k} &= \hat{\psi}_{b_{k+1}}^{b_k} + \frac{1}{t_{k+1} - t_k}(J_{b_a}^{\psi} \delta b_{a_k} + J_{b_w}^{\psi} \delta b_{w_k}) \\ (where \; J_{b_w}^{\alpha} &= \frac{\partial \alpha_{b_{k+1}}^{b_k}}{\partial b_{w_k}}, J_{b_w}^{\beta} = \frac{\partial \beta_{b_{k+1}}^{b_k}}{\partial b_{w_k}}, J_{b_a}^{\psi} = \frac{\partial \psi_{b_{k+1}}^{b_k}}{\partial b_{a_k}}, \\ J_{b_w}^{\psi} &= \frac{\partial \psi_{b_{k+1}}^{b_k}}{\partial b_{w_k}}) \end{aligned} \tag{17}$$

Consequently, an external force residual is constructed based on the previously calculated preintegration, propagation, and bias corrections. It is composed as in (18), and the corresponding term is integrated through (9).

$$r_F^k = \begin{bmatrix} \alpha_{b_{k+1}}^{b_k} - \hat{\alpha}_{b_{k+1}}^{b_k} \\ \beta_{b_{k+1}}^{b_k} - \hat{\beta}_{b_{k+1}}^{b_k} \\ \psi_{b_{k+1}}^{b_k} - \hat{\psi}_{b_{k+1}}^{b_k} \\ b_{a_{k+1}} - b_{a_k} \end{bmatrix} \tag{18}$$

IV. SIMULATION

A. Simulation environment setup

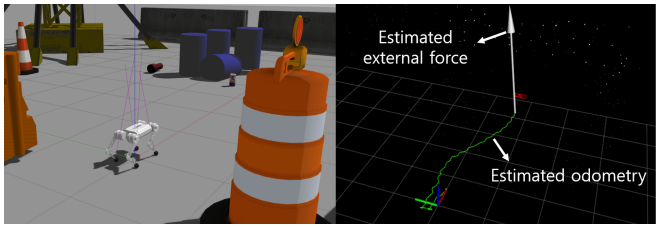

Fig. 2: Simulation process. Left: gazebo environment, Right: visualized trajectory and external forces

The simulation was implemented in the Gazebo environment to verify the performance of the proposed estimator. A mini cheetah robot [17] is used for a simulation, and whole dynamics are configured based on the physical quantity of each robot link. The sensors IMU, joint encoder, and torque are updated at 200 Hz, and the stereo camera has a 30 Hz rate. The controller and environment used for simulation are based on [18]. We used a PC with Intel Core i7-1165G7 CPU and 32GB memory, and tested the proposed method on Ubuntu 18.04/ROS melodic.

To confirm the performance of the proposed DOB-based ground reaction force estimator, we compared the force sensor attached to the tip of the robot, the value obtained through whole dynamics, and the value obtained using the DOB with whole dynamics. For comparison, we assumed the force sensor to be the ground truth.

For external force estimation, we divide the standing situation and the walking situation. Step input applied to the robot with amplitudes of 35N (x-axis), 15N (y-axis), 120N (z-axis) when standing. During walking, sinusoidal external forces in each direction were sequentially applied, and the maximum magnitude was 40N (x-axis), 40N (y-axis), and 120N (z-axis), respectively.

V. RESULTS

A. Estimation of the ground reaction force

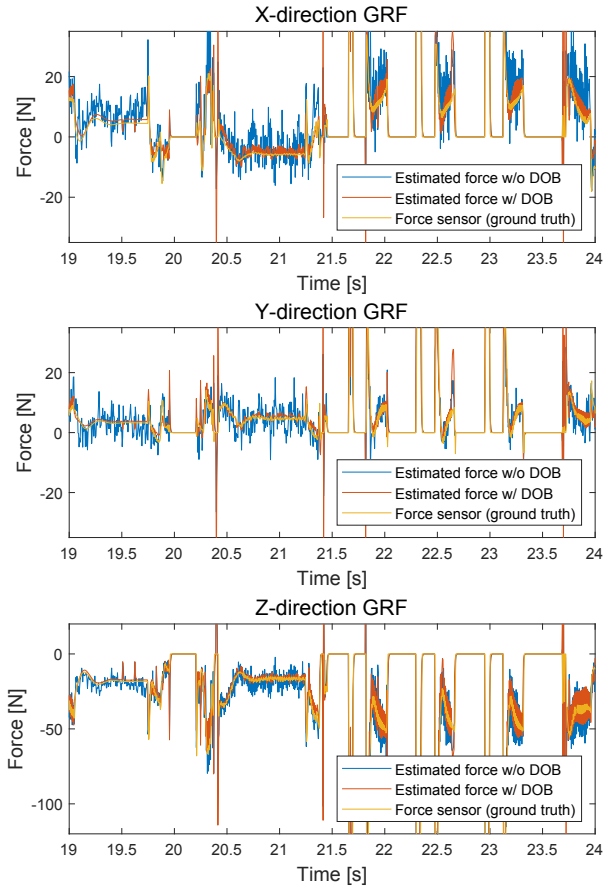

Fig. 3: Comparison results of estimating the ground reaction force (GRF) of the front left leg.

As shown in Fig. 3, when estimating the force only

through dynamics without using the DOB, the result is very noisy due to $\ddot{q}$. On the other hand, when the DOB is used together with the robot dynamics, the noise is significantly reduced. We finally conclude that the DOB can improve the force estimation performance of each foot.

B. Estimation of the external force

In this section, we confirmed the estimation performance of the external force using factor graph optimization based on the previously obtained ground reaction forces. Since the movement of the quadruped robot is largely divided into a standing (all feet are in contact) and a walking state (contact conditions are changed constantly), simulations were implemented in each case. For analysis, a naive approach obtained by passing a low pass filter through $F_{ext} = Ma - \sum_{i=1}^{4} F_{leg,i}$, and the values estimated using a factor graph (with the DOB and without the DOB) were compared.

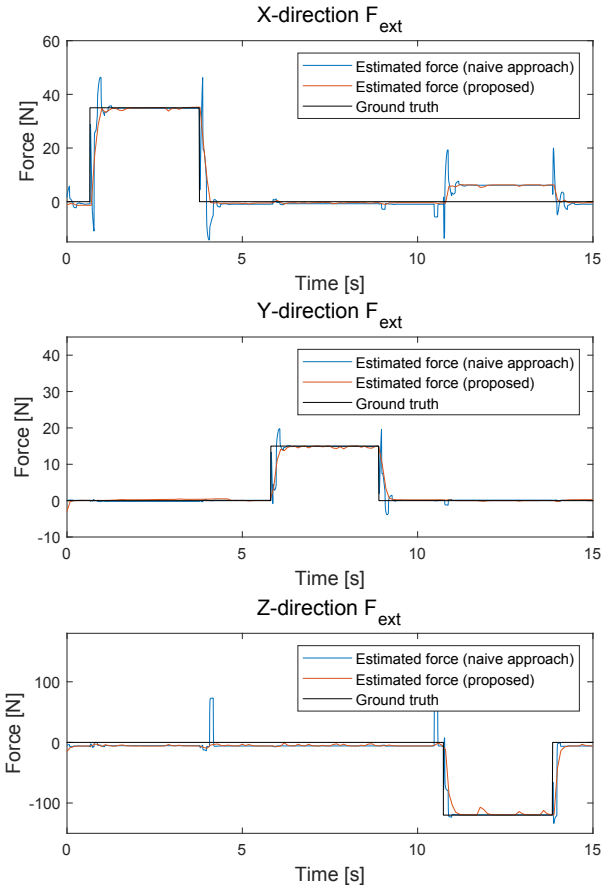

Fig. 4: Estimation results of the external force during standing. The force was applied within the range where the robot did not fall ($F_x = 35N, F_y = 15N, F_z = 120N$).

When the robot is standing, the movement is relatively slow, and the joint acceleration, which was a problem before, is also close to 0; thus, we do not compare the cases with or without the DOB. Therefore, the factor graph-based approach and the naive approach were compared. Fig. 4 shows that the external force is estimated well in both cases. However, in the naive approach, peak value occurs in several regions, whereas the proposed method shows a more stable estimation result. Additionally, we can see that each axis force affects the other axes. This problem occurs as a result of the assumption that the center of gravity of the whole system is the base center. A moment is generated due to the deviation from the actual center of gravity, which affects other axes. This issue can be resolved through more precise modeling in the future.

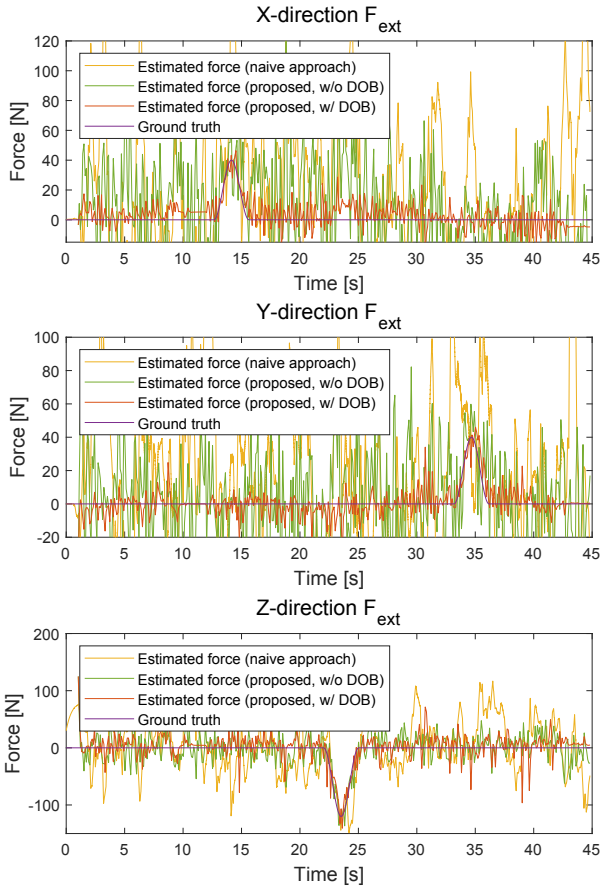

Fig. 5: Estimation results of the external force during walking. Similar to the standing case, the force was applied within the range where the robot did not fall. Shifted sine wave applied to the robot (amplitude: $F_x = 40N, F_y = 40N, F_z = 120N$). In particular, in the z-axis, where all three methods estimate well, the RMSE error and standard deviation of the proposed method were reduced by 49.49% and 51.53% compared to the naive approach.

On the other hand, in walking motion, the contact conditions change constantly, and the impact and slip occur at the end effector. Therefore, the estimation performance is inevitably lower than that in the standing case. The results are shown in Fig. 5. All three methods estimated the shape and amplitude of the external force quite well in the z-direction (a relatively large force was applied). Moreover, when the DOB and factor graph approaches were used together, the highest performance was obtained. In the x-axis and y-axes, in which the magnitude of the external force is small, the noise value is relatively conspicuous. As a result, it seems almost impossible to estimate small-magnitude forces other

than the proposed method.

C. Pose estimation comparison with VINS-Fusion

The method presented in this paper estimates the pose and external force of the robot simultaneously by adding force-related factors to the existing VIO. This new force residual can affect the existing VIO because it is optimized together with robot poses. So it is necessary to check the change in pose estimation performance before and after the addition of new terms. Therefore, the estimation results of the pose were compared and analyzed. (obtained by rpg trajectory evaluation tool [19]). In Fig. 6, there is no significant difference in the path depending on whether the force estimate term is added. However, as shown in Fig. 7, the translation error slightly increased, which seems to be a trade-off that occurred while simultaneously performing force estimation.

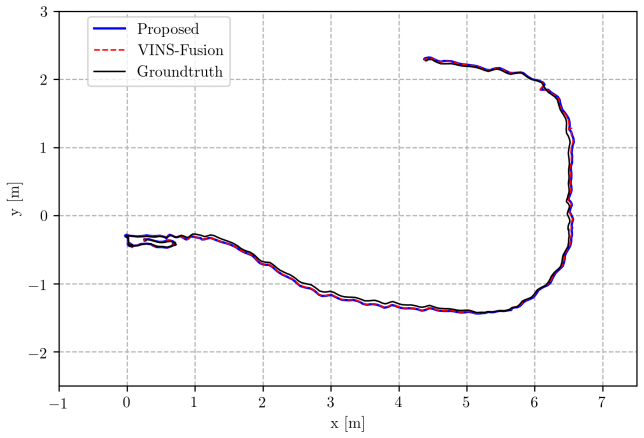

Fig. 6: Top view of estimated trajectory comparison (VINS-Fusion: red dot line, Proposed: blue line).

VI. CONCLUSIONS

In this paper, external forces were estimated without an end effector force sensor through whole dynamics, a disturbance observer, and a factor graph framework. Before estimating the external force, dynamics were used to calculate the leg force of the robot, and a more accurate value was obtained by using the DOB to depress the large noise generated from the joint acceleration. Next, an external force residual was added through the preintegration method to the existing VIO system. The proposed method showed relatively good estimation performance despite slip, impact and encoder noise. In addition, the performance change of the pose estimation was also compared and analyzed (with and without a force residual).

In this study, the estimation was performed only when an external force acts on the center of the base, but in other cases, the moment also occurs, resulting in additional estimation variables. However, it is expected that 6 DOF forces and moments can be estimated without difficulty if only the equations and estimation variables are appropriately added. In the future, the estimated force can be transmitted

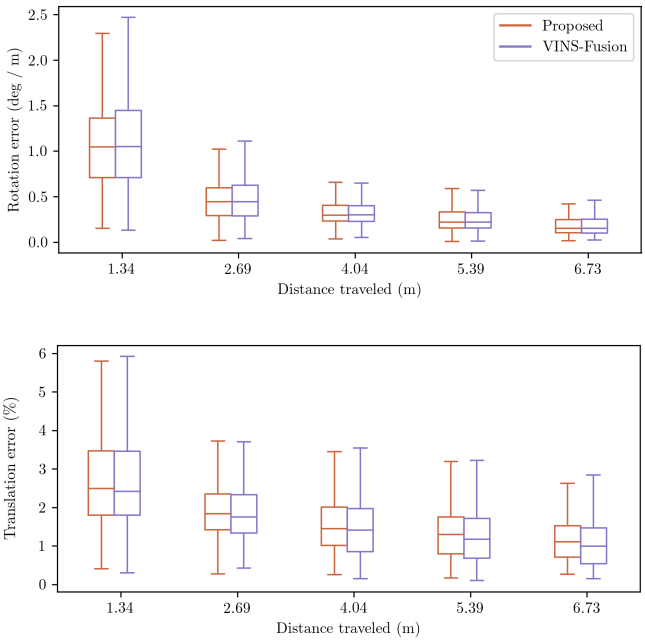

Fig. 7: RMSE boxplot of the translation and rotation error. VINS-Fusion and the proposed methods are compared. The rotation error is almost the same, but the translation error is slightly increased.

to the controller and applied for recovery or interaction with the environment to finally obtain robust movements.

REFERENCES

[1] M. Bloesch, M. Hutter, M. A. Hoepflinger, S. Leutenegger, C. Gehring, C. D. Remy, and R. Siegwart, "State estimation for legged robots-consistent fusion of leg kinematics and imu," *Robotics*, vol. 17, pp. 17–24, 2013.

[2] S. Teng, M. W. Mueller, and K. Sreenath, "Legged robot state estimation in slippery environments using invariant extended kalman filter with velocity update," in *2021 IEEE International Conference on Robotics and Automation (ICRA)*. IEEE, 2021, pp. 3104–3110.

[3] R. Hartley, M. G. Jadidi, J. W. Grizzle, and R. M. Eustice, "Contact-aided invariant extended kalman filtering for legged robot state estimation," *arXiv preprint arXiv:1805.10410*, 2018.

[4] J. Hu and R. Xiong, "Contact force estimation for robot manipulator using semiparametric model and disturbance kalman filter," *IEEE Transactions on Industrial Electronics*, vol. 65, no. 4, pp. 3365–3375, 2017.

[5] S. A. Fakoorian, D. Simon, H. Richter, and V. Azimi, "Ground reaction force estimation in prosthetic legs with an extended kalman filter," in *2016 Annual IEEE Systems Conference (SysCon)*. IEEE, 2016, pp. 1–6.

[6] A. Wahrburg, E. Morara, G. Cesari, B. Matthias, and H. Ding, "Cartesian contact force estimation for robotic manipulators using kalman filters and the generalized momentum," in *2015 IEEE International Conference on Automation Science and Engineering (CASE)*. IEEE, 2015, pp. 1230–1235.

[7] T. Qin, P. Li, and S. Shen, "Vins-mono: A robust and versatile monocular visual-inertial state estimator," *IEEE Transactions on Robotics*, vol. 34, no. 4, pp. 1004–1020, 2018.

[8] C. Campos, R. Elvira, J. J. G. Rodríguez, J. M. Montiel, and J. D. Tardós, "Orb-slam3: An accurate open-source library for visual, visual–inertial, and multimap slam," *IEEE Transactions on Robotics*, vol. 37, no. 6, pp. 1874–1890, 2021.

[9] C. Forster, L. Carlone, F. Dellaert, and D. Scaramuzza, "Imu preintegration on manifold for efficient visual-inertial maximum-a-posteriori estimation." Georgia Institute of Technology, 2015.

[10] R. Hartley, J. Mangelson, L. Gan, M. G. Jadidi, J. M. Walls, R. M. Eustice, and J. W. Grizzle, "Legged robot state-estimation through combined forward kinematic and preintegrated contact factors," in

2018 IEEE International Conference on Robotics and Automation (ICRA). IEEE, 2018, pp. 4422–4429.

[11] D. Wisth, M. Camurri, and M. Fallon, "Preintegrated velocity bias estimation to overcome contact nonlinearities in legged robot odometry," in *2020 IEEE International Conference on Robotics and Automation (ICRA)*. IEEE, 2020, pp. 392–398.

[12] B. Nisar, P. Foehn, D. Falanga, and D. Scaramuzza, "Vimo: Simultaneous visual inertial model-based odometry and force estimation," *IEEE Robotics and Automation Letters*, vol. 4, no. 3, pp. 2785–2792, 2019.

[13] Z. Ding, T. Yang, K. Zhang, C. Xu, and F. Gao, "Vid-fusion: Robust visual-inertial-dynamics odometry for accurate external force estimation," in *2021 IEEE International Conference on Robotics and Automation (ICRA)*. IEEE, 2021, pp. 14 469–14 475.

[14] M. Fourmy, T. Flayols, P.-A. Léziart, N. Mansard, and J. Solà, "Contact forces preintegration for estimation in legged robotics using factor graphs," in *2021 IEEE International Conference on Robotics and Automation (ICRA)*. IEEE, 2021, pp. 1372–1378.

[15] A. Mohammadi, M. Tavakoli, H. J. Marquez, and F. Hashemzadeh, "Nonlinear disturbance observer design for robotic manipulators," *Control Engineering Practice*, vol. 21, no. 3, pp. 253–267, 2013.

[16] J. Sola, "Quaternion kinematics for the error-state kalman filter," *arXiv preprint arXiv:1711.02508*, 2017.

[17] B. Katz, J. Di Carlo, and S. Kim, "Mini cheetah: A platform for pushing the limits of dynamic quadruped control," in *2019 international conference on robotics and automation (ICRA)*. IEEE, 2019, pp. 6295–6301.

[18] J. M. Jimeno, "Champ," Accessed on: Sep. 14, 2022. [Online]. Available: http://https://github.com/chvmp/champ.

[19] Z. Zhang and D. Scaramuzza, "A tutorial on quantitative trajectory evaluation for visual (-inertial) odometry," in *2018 IEEE/RSJ International Conference on Intelligent Robots and Systems (IROS)*. IEEE, 2018, pp. 7244–7251.